



## RESEARCH ARTICLE

10.1002/2016JB013350

## Key Points:

- Median cryptotephra shard size varies by a relatively small amount even over distances of hundreds to thousands of kilometers
- There is no simple relationship between median shard size and transport distance due to the dynamic controls on cryptotephra transport
- Cryptotephra shard size distributions are recorded differently in lakes and peatlands in close proximity (<10 km distant)

## Supporting Information:

- Supporting Information S1
- Table S1

## Correspondence to:

E. J. Watson,  
e.j.watson@outlook.com

## Citation:

Watson, E. J., G. T. Swindles, J. A. Stevenson, I. Savov, and I. T. Lawson (2016), The transport of Icelandic volcanic ash: Insights from northern European cryptotephra records, *J. Geophys. Res. Solid Earth*, 121, 7177–7192, doi:10.1002/2016JB013350.

Received 11 JUL 2016

Accepted 2 OCT 2016

Accepted article online 5 OCT 2016

Published online 30 OCT 2016

©2016. The Authors.

This is an open access article under the terms of the Creative Commons Attribution License, which permits use, distribution and reproduction in any medium, provided the original work is properly cited.

## The transport of Icelandic volcanic ash: Insights from northern European cryptotephra records

E. J. Watson<sup>1</sup>, G. T. Swindles<sup>1</sup>, J. A. Stevenson<sup>1,2,3</sup>, I. Savov<sup>2</sup>, and I. T. Lawson<sup>3</sup>

<sup>1</sup>School of Geography, University of Leeds, Leeds, UK, <sup>2</sup>School of Earth and Environment, University of Leeds, Leeds, UK, <sup>3</sup>Department of Geography and Sustainable Development, University of St. Andrews, St. Andrews, UK

**Abstract** Fine ash produced during volcanic eruptions can be dispersed over a vast area, where it poses a threat to aviation, human health, and infrastructure. We analyze the particle size distributions, geochemistry, and glass shard morphology of 19 distal (>1000 km from source) volcanic ash deposits distributed across northern Europe, many geochemically linked to a specific volcanic eruption. The largest glass shards in the cryptotephra deposits were 250  $\mu\text{m}$  (longest axis basis). For the first time, we examine the replicability and reliability of glass shard size measurements from peatland and lake archives. We identify no consistent trend in the vertical sorting of glass shards by size within lake and peat sediments. Measuring the sizes of 100 shards from the vertical sample of peak shard concentration is generally sufficient to ascertain the median shard size for a cryptotephra deposit. Lakes and peatlands in close proximity contain cryptotephra with significantly different median shard size in four out of five instances. The trend toward a greater amount of larger shards in lakes may have implications for the selection of distal sites to constrain the maximum glass shard size for modeling studies. Although the 95th percentile values for shard size generally indicate a loss of larger shards from deposits at sites farther from the volcano, due to the dynamic nature of the controls on tephra transport even during the course of one eruption there is no simple relationship between median shard size and transport distance.

### 1. Introduction

During explosive volcanic eruptions ( $\geq 3$  volcanic explosivity index (VEI) [Newhall and Self, 1982]) “extremely fine” ash (<64  $\mu\text{m}$ ) can be transported over long distances [Rose and Durant, 2011; Lane et al., 2013]. In low concentrations volcanic ash poses a small risk to human health, but fine ash can be a hazard for modern aviation [Folch, 2012]. Understanding the nature of past volcanic ash clouds can inform our understanding of the risk posed by future events.

Volcanic eruptions which produce a significant amount of fine ash over northern Europe have occurred with a mean return interval of  $56 \pm 9$  years over the last 1000 years [Swindles et al., 2011, 2013b]. However, there is a lack of data on the particle size distribution of such volcanic ash reaching northern Europe. The geological record offers a source of information on distal (>1000 km) ash fallout. Cryptotephra deposits from past ash clouds are stored in over 120 peatlands and lakes across northern Europe [Lawson et al., 2012]. As cryptotephra form spatially widespread, isochronous horizons, they are widely used for correlating geological records (“tephrostratigraphy”) [Lowe, 2011]. Cryptotephra deposits in the geological record typically span a few centimeters in depth [Davies et al., 2007; Payne and Gehrels, 2010]. Volcanic glass shards are often counted for the purpose of identifying the depth of the peak shard concentration, which typically represents the isochron widely used in tephrochronology. However, the sizes and shapes of shards are rarely reported.

Recent work has indicated that the particle size distributions of cryptotephra can be used to evaluate the satellite infrared methods often used to monitor volcanic ash clouds [Stevenson et al., 2015]. Furthermore, the particle size distributions of distal tephra occurrences can provide more realistic estimates of total erupted tephra volumes [Ponomareva et al., 2015] that are currently biased toward tephra, which falls out closer to the volcano. However, there has been no study into how representative particle size distributions from cryptotephra deposits in lakes and peatlands are of ash fallout over a region. Raised peatlands are commonly considered to be archives of primary fallout material, whereas tephra in lakes might have fallen elsewhere in the catchment and been subject to a greater amount of reworking [Davies et al., 2007]. The movement of shards across the terrestrial surface following deposition, and vertical movement in peat and lake sediments, might cause the sorting of glass shards of different sizes, or even lead to the fragmentation

of the glass shards before they enter the geological record, resulting in a particle size distribution in the geological record which does not reflect the particle size distribution of ash fallout over the site. Furthermore, there is no indication as to how many glass shards must be measured in order to reliably estimate the particle size distribution for a site. Before cryptotephra particle size distributions can be applied more widely as records of ash clouds, these methodological issues must be understood.

The overall aim of this paper is to understand the extent to which the particle size distribution and shard morphology of cryptotephra deposits can be used to provide information about the nature (e.g., plume height) of the eruptions which produced them. We analyze the particle size distribution and shard morphology of cryptotephra deposits from 14 sites in northern Europe. We examine whether cryptotephra particle size distributions in lakes and peatlands are likely to reflect cryptotephra fallout over the region or whether they are confounded by the sorting of glass shards in the catchment or across the peatland. Finally, we assess whether probabilistic modeling can be used to estimate eruption parameters based on cryptotephra particle size distributions in the geological record.

We test the following hypotheses:

1. Shard sizes will vary significantly between different cores from the same peatland site (glass shards will be reworked on the peatland surface according to size).
2. The median shard size for the same cryptotephra deposit will be significantly different in lakes and peatlands which have received the same primary tephra-fall deposits.
3. There is no stratigraphic variation in the particle size distribution of a cryptotephra deposit (i.e., above, on, or below the peak shard concentration) because particle size does not significantly alter the movement of particles vertically through peat or lake sediments.
4. The median shard size will decrease with increased distance between the fallout site and the volcanic source.

## 2. Methods

### 2.1. The Geological Record

#### 2.1.1. Field Sampling

Sites were selected in order to span a range of distances from Iceland, the main source region for cryptotephra deposits in northern Europe (Figure 1). For the purposes of this study the distances from Iceland to each site are the great circle distance between Hekla volcano, the dominant source of Holocene cryptotephra in northern Europe, and the site location (Table 1). Table 1 also contains references for detailed site descriptions. Peatlands in this study are predominantly ombrotrophic and therefore would be expected to record only primary tephra-fall material. All of the lakes in this study lie in small, natural basins and with water depths not exceeding 4 m at the time of sampling [cf. *Watson et al.*, 2016]. With the exception of Malham Tarn, which is fed by natural springs, all lakes are stream fed. To examine possible differences in the particle size distribution of the same tephra in both peatlands and lakes, at four sites (Sammakovuoma and Degerö Stormyr /Lake Svartkälstjärn in Sweden, Claraghmore in northern Ireland, and Malham in England) we sampled both a lake and a peatland in close proximity (<10 km apart). Cores were extracted using a Russian-type corer [Jowsey, 1966], following the parallel hole method [De Vleeschouwer *et al.*, 2011]. With the exception of Fallahogy peatland, where multiple cores were retrieved [cf. *Watson et al.*, 2015], one core was extracted from each site.

#### 2.1.2. Tephra Analysis

Cores were examined in 5 cm<sup>3</sup> contiguous samples. Where cryptotephra was identified, the cores were resampled at 1 cm intervals to identify the location of the peak shard concentration. Samples from ombrotrophic peatlands were prepared using the method outlined by *Hall and Pilcher* [2002] and *Swindles et al.* [2010]. Samples containing minerogenic material (which occurred in all lake cores and in the samples from the Swedish peatlands) were extracted using heavy density liquid flotation (cleaning float 2.25 g cm<sup>-3</sup>, retaining float 2.5 g cm<sup>-3</sup>) [Blockley *et al.*, 2005]. For both methods, sieving of samples through a 10 μm mesh was necessary to remove detrital material. Therefore, excluding the samples from Unst which were sieved at 20 μm, the minimum particle size analyzed in this study is that retained by a 10 μm mesh.

Shards were mounted onto slides using Histomount and examined at 200–400× magnification. Shards from one eruption typically have a vertical span of a few centimeters in lake and peatland records [Davies *et al.*, 2007].

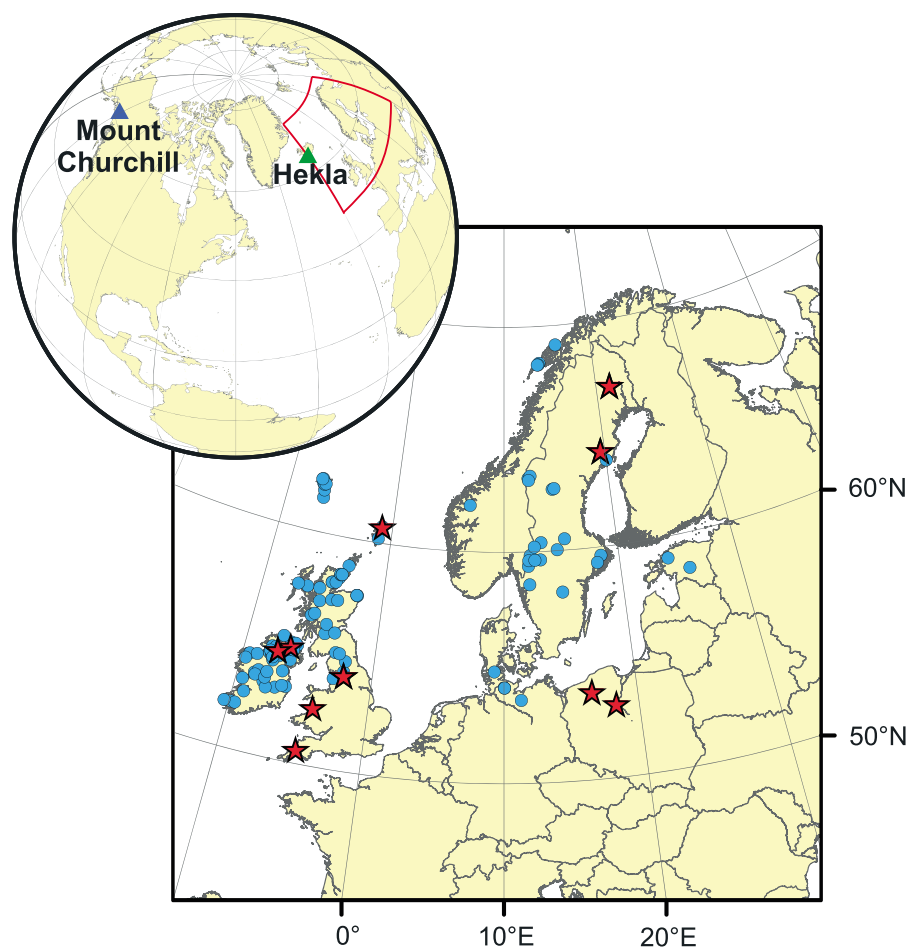


**Figure 1.** The distribution of sites where Holocene cryptotephra deposits have been identified. The blue circles indicate the lake and peatland sites where glass shards in cryptotephra have been geochemically analyzed [Lawson *et al.*, 2012]. The stars indicate the sites where glass shards in cryptotephra have been geochemically analyzed and where shard size analyses have been conducted. The globe indicates the location of two source volcanoes for cryptotephra identified in this study, Mount Churchill, Alaska, and the Hekla volcano, the source of the majority of the Holocene cryptotephra deposits in northern Europe.

Therefore, all samples within each vertical cryptotephra spread were examined, not only the peak sample. The low shard count totals for each eruptive (typically tens to hundreds of shards) in distal records provided insufficient quantities of shards for automated analysis of shard size/shape by laser granulometer or Coulter counter (<1 g). Therefore, shards were identified and measured using an eyepiece graticule. Shard size was measured in two dimensions: (i) the length of the longest axis (max A), referred to as “shard size” unless otherwise stated, and (ii) the maximum width at 90° to the first measurement (max B). Aspect ratio was calculated as max A divided by max B.

Glass shards were extracted for geochemistry using two established methods. In peat with little minerogenic material, extraction was by acid digestion [Dugmore and Newton, 1992]. Samples were treated with conc. HNO<sub>3</sub> and H<sub>2</sub>SO<sub>4</sub> acids before sieving the residue at 10 μm and rinsing thoroughly with distilled water. Samples with larger amounts of minerogenic material were extracted by density separation.

Samples were either mounted onto glass slides [Dugmore and Newton, 1992] or mounted into blocks [Hall and Hayward, 2014]. All samples were polished to a 0.25 μm finish. The majority of geochemical data was obtained via electron probe microanalysis at the University of Edinburgh Tephra Analytical Unit. A beam size of 5 μm was used throughout, and beam current was varied during each analysis to limit volatile losses [Hayward, 2012]. All analyses were conducted at 15 kV with beam currents of 2 nA (Na, Mg, Al, Si, K, Ca, and Fe)

**Table 1.** The Location of Each Site and the Cryptotephra Deposits Identified<sup>a</sup>

Site (Peatland/Lake)	Location	Reference	Distance from Hekla (km)	Hekla 4	Hekla 1104	Hekla 1158	A.D. 860 B	SN-1	Glen Garry	MOR-T4	
Shetland Underhoull (P)	Shetland	60.719°N 0.948°W	<i>Swindles et al. [2013a]</i>	1075	1	1	1				
Claraghmore bog (P)	Ireland	54.633°N 7.454°W	<i>Watson et al. [2016]</i>	1246	1		1			1	
Claraghmore Lake (L)	Ireland	54.631°N 7.450°W	<i>Watson et al. [2016]</i>	1246							
Fallahogy (P)	Ireland	54.911°N 6.557°W	<i>Watson et al. [2015]</i>	1247							
Malham Moss (P)	England	54.097°N 2.173°W	<i>Watson et al. [2016]</i>	1478	1				1		
Malham Tarn (L)	England	54.096°N 2.165°W	<i>Watson et al. [2016]</i>	1478					1		
Cors Fochno (P)	Wales	52.504°N 4.012°W	<i>Watson [2016]</i>	1563						1	
Bodmin (P)	England	50.589°N 4.625°W	<i>Watson [2016]</i>	1733			1				
Degerö Stormyr (P)	Sweden	64.181°N 19.564°E	<i>Watson et al. [2016]</i>	1878	1	1	1				
Lake Svartkälstjärn (L)	Sweden	64.264°N 19.552°E	<i>Watson et al. [2016]</i>	1878	1	1	1				
Sammakovuoma lake (L)	Sweden	66.992°N 21.500°E	<i>Watson et al. [2016]</i>	1891	1	1			1		
Sammakovuoma bog (P)	Sweden	66.995°N 21.457°E	<i>Watson et al. [2016]</i>	1891		1			1		
Kusowskie Bagno (P)	Poland	53.816°N 16.588°E	<i>Watson [2016]</i>	2326			1				
Linje (P)	Poland	53.187°N 18.309°E	<i>Watson [2016]</i>	2457							
			Total		6	5	3	3	2	2	2

<sup>a</sup>Lake and peatland pairs in close proximity are highlighted in grey. Sites are ordered by increasing distance from the Hekla volcano. Cryptotephra deposits that have not been attributed to an Icelandic source eruption (Glen Garry, QUB 384 G3-4), or which have been attributed to an alternative source region (e.g., Alaska; A.D. 860 B), are shown in italics.

or 80 nA (P, Ti, and Mn). Secondary glass standards were analyzed before and after analysis runs of unknown glass shards. Analyses for glass from Malham Moss tephra and some of the Unst samples were conducted at the University of Leeds on a JEOL8230 electron microprobe using a beam current of 10 nA and a 10  $\mu$ m beam. Assignments to eruptive event were based on stratigraphy and comparison of glass major element geochemistry with that of the European tephra geochemistry database "TephraBase" [Newton et al., 2007] and published literature.

## 2.2. Statistical Analysis

The majority of statistical analysis was conducted in Minitab 17. Unless otherwise stated, significance is defined as the 95% significance level ( $p < 0.05$ ). Bootstrap analysis was conducted in R version 3.1.0., in each instance analysis included 10,000 iterations, random sampling with replacement. The Unst tephra was sieved at 20  $\mu$ m [Swindles et al., 2013a], and therefore, during comparisons of the shard size distributions of cryptotephra deposits from the Unst site with those from other sites, we excluded shards  $< 20 \mu$ m from the analysis.

## 2.3. Modeling Cryptotephra Fallout

In order to assess whether probabilistic modeling can be used to estimate eruption parameters based on cryptotephra (i.e., glass shard) particle size distributions in the geological record, we develop and test a simple probabilistic model of cryptotephra fallout. One of the major challenges in modeling tephra fallout from past volcanic eruptions is uncertainty in model input parameters. Basic model input parameters such as plume height and wind speed are often poorly constrained or completely unknown for prehistoric eruptions. In these instances a stochastic approach, whereby input parameters are sampled from probability density functions, allows for an assessment of various scenarios [Bonadonna et al., 2005]. We developed a simple probabilistic model which calculates the terminal velocity and thus the distance travelled and fallout time for glass shards released during a volcanic eruption. The model consists of two parts, a physical submodel which calculates the distance travelled by each particle based on input parameters including plume height, wind speed, and particle size and a stochastic submodel which is used to sample input parameters for the physical model from probability density functions to forecast a variety of conceivable outcomes. Full details of the model are given in Text S1 and Figure S1 in the supporting information. The model was tested against empirical fallout data from the eruption of Mount St. Helens in 1980 [Carey and Sigurdsson, 1982].

Probability density functions (PDFs) for plume height, sphericity [cf. Ganser, 1993], and wind speed were constructed based on empirical observations and previous published literature [Alfano et al., 2011; Bonadonna and Phillips, 2003] (Table 2). Plume height is sampled from a log uniform distribution truncated at 4 km

**Table 1.** (continued)

Site (Peatland/Lake)	Askja 1875	Lairg A	Lairg B	Hekla 1947	Hekla 1845	Hekla 1510	Öræfajökull 1362	Microlite/ GB4-150	CLA-L1 Grímsvötn?	Hekla-S/ Kebister	Hekla 3	QUB_384 _G3/G4	A.D. 860 A
Shetland Underhoull (P)										1			
Claraghmore bog (P)							1	1					
Claraghmore Lake (L)		1	1						1				
Fallahogy (P)				1	1	1							
Malham Moss (P)		1	1										
Malham Tarn (L)													
Cors Fochno (P)				1	1							1	
Bodmin (P)													1
Degerö Stormyr (P)	1										1		
Lake Svartkälstjärn (L)													
Sammakovuoma lake (L)													
Sammakovuoma bog (P)													
Kusowskie Bagno (P)													
Linje (P)	1												
Total	2	2	2	2	2	1	1	1	1	1	1	1	1

and 35 km. Although there is some evidence for the transport of fine glass shards from plume heights < 4 km [Stevenson *et al.*, 2013], shards released at such low altitudes are likely to represent a negligible proportion of the shards contained in northern European cryptotephra records. Explosive eruptions associated with plume heights exceeding 30 km do not occur frequently in Iceland. However, to account for eruptions such as that of Askja in 1875 (VEI 5, plume height ~35 km), we set 35 km as the maximum plume height. The log distribution reflects the bias toward a higher frequency of low-magnitude eruptions with lower plume heights [Simkin and Siebert, 1994]. Wind speed is sampled from a normal distribution based on the average wind speed values between 0 and 48 km height as reported by Lacasse [2001] and maximum and minimum wind speed values of 10–30 ms<sup>-1</sup>. Examples of values sampled from each of the above PDFs are given in Figure S2.

Particle aggregation and precipitation can promote the early fallout of atmospheric particles [Mattsson and Vesanen, 1988; Durant *et al.*, 2009]. However, we do not account for aggregation or the impact of precipitation, as the processes controlling the aggregation of particles are not well parameterized [Brown *et al.*, 2012]. We also do not take into account the particle size distribution at source [Beckett *et al.*, 2015]; instead, the model is run for a given glass shard size. The model also does not include transport of glass shards while they are suspended in the turbulent spreading plume.

### 3. Results

#### 3.1. Maximum Shard Size

To estimate the number of shard measurements required to assess the median shard size ( $\pm 5 \mu\text{m}$ ) for a sample within a 95% confidence window, we conducted bootstrap reanalysis of shard size measurements from cryptotephra deposits containing large numbers of shards. Our analysis indicates that around 100 shard measurements is generally sufficient (Figure S3). Therefore, for the purposes of this study, a minimum of 100 shards was measured in each sample; where samples contained <100 shards the maximum number of shards possible was counted. The shard sizes of over 9500 shards from 20 different cryptotephtras were measured (Table S1 in the supporting information).

The geochemistry of the glass shards in the cryptotephtras ranged from basaltic to andesitic, dacitic, trachydacitic, and rhyolitic (Figure 2). The majority of deposits could be geochemically correlated to Icelandic eruptives. However, three cryptotephtras contain glass shards with a major element geochemistry which does not match the geochemistry of glass in tephra from Icelandic eruptions; for two of these cryptotephtras the source region therefore remains unknown (Glen Garry [Dugmore *et al.*, 1995] and QUB 384-G3-G4 [Pilcher *et al.*, 2005]). Glass shards from the third non-Icelandic cryptotephtra match the major element geochemistry of glass shards from the A.D. 860 B tephra, correlated to the White River Ash east (WRAe) from the Bona-Churchill massif, Alaska

**Table 2.** Model Parameters and Input Values (or Ranges) Used in the Tephra Fallout Model

Model Parameter (Units)	Input Value (or Range)	Reference
<b>Atmospheric properties</b>		
Air viscosity (Pa s)	$1.78 \times 10^{-5}$	Stevenson et al. [2015]
Air density ( $\text{kg m}^{-3}$ )	Varies with height according to the equation of Connor et al. [2013]	Connor et al. [2013]
<b>Particle properties</b>		
Size/diameter ( $\mu\text{m}$ )	Specified by user (0–250 $\mu\text{m}$ )	
Density ( $\text{kg m}^{-3}$ )	Varies with particle size (~2300–1900 $\text{kg m}^{-3}$ )	Bonadonna and Phillips [2003]
Shape (sphericity, dimensionless)	Sampled from probability density function. Normal distribution: mean = 0.8, standard deviation = 0.1	Alfano et al. [2011]
<b>Release properties</b>		
Release height (km)	Sampled from a probability density function. Log-uniform distribution: maximum = 35 km, minimum = 4 km, smaller plume heights more likely	Bonadonna et al. [2005]
<b>Meteorology</b>		
Wind speed ( $\text{m s}^{-1}$ )	Sampled from a probability density function. Truncated normal distribution mean = 17.4, standard deviation = 4, minimum = 10, maximum = 30	Lacasse [2001]
Gravity ( $\text{m s}^{-2}$ )	9.81	

[Jensen et al., 2014]. Only the 17 cryptotephra with a known or suggested source eruption in Iceland are included in subsequent analyses concerning shard size of a tephra with distance from source.

In agreement with Stevenson et al. [2015], in both lake and peatland records, the majority of particle size distributions exhibit a lognormal distribution, with a tail of larger shards. Median shard size varied between 35 and 75  $\mu\text{m}$  (median = 51  $\mu\text{m}$ ; Figure 3). The largest measured shard size (max A) was 250  $\mu\text{m}$ , indicating that shards typically considered large in the context of cryptotephra deposits can be transported long

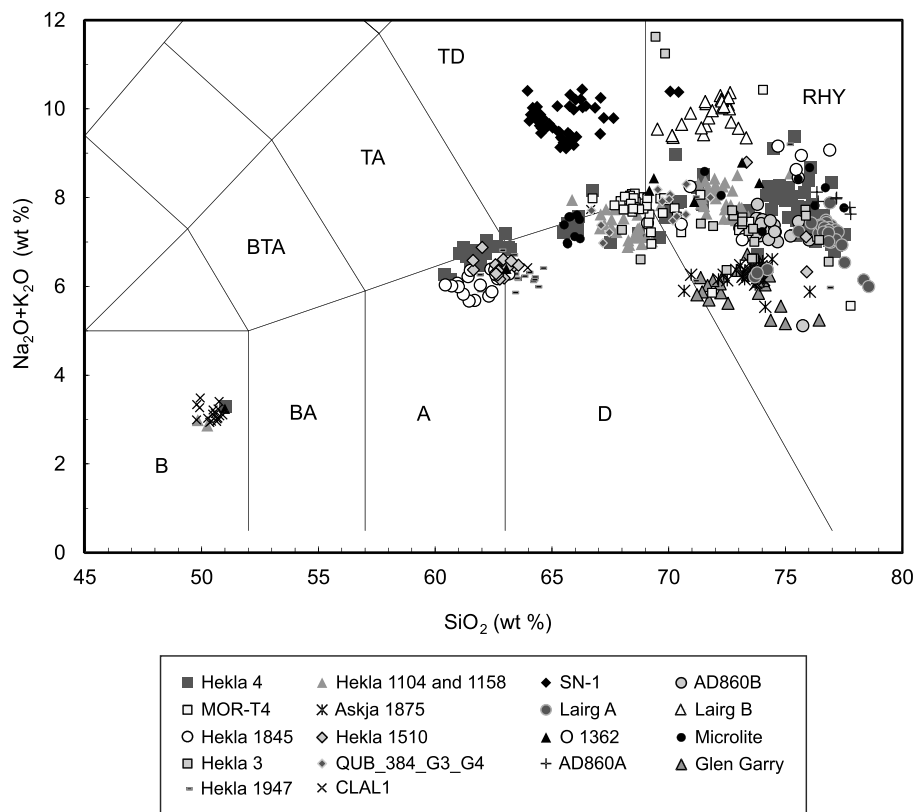


**Figure 2.** The partial major element compositions of glass shards from cryptotephra deposits in this study. Annotations follow standard terminology, e.g., RHY = rhyolite, D = dacite, and A = andesite [Le Maitre et al., 1989]. O 1362 = Örfajökull 1362.

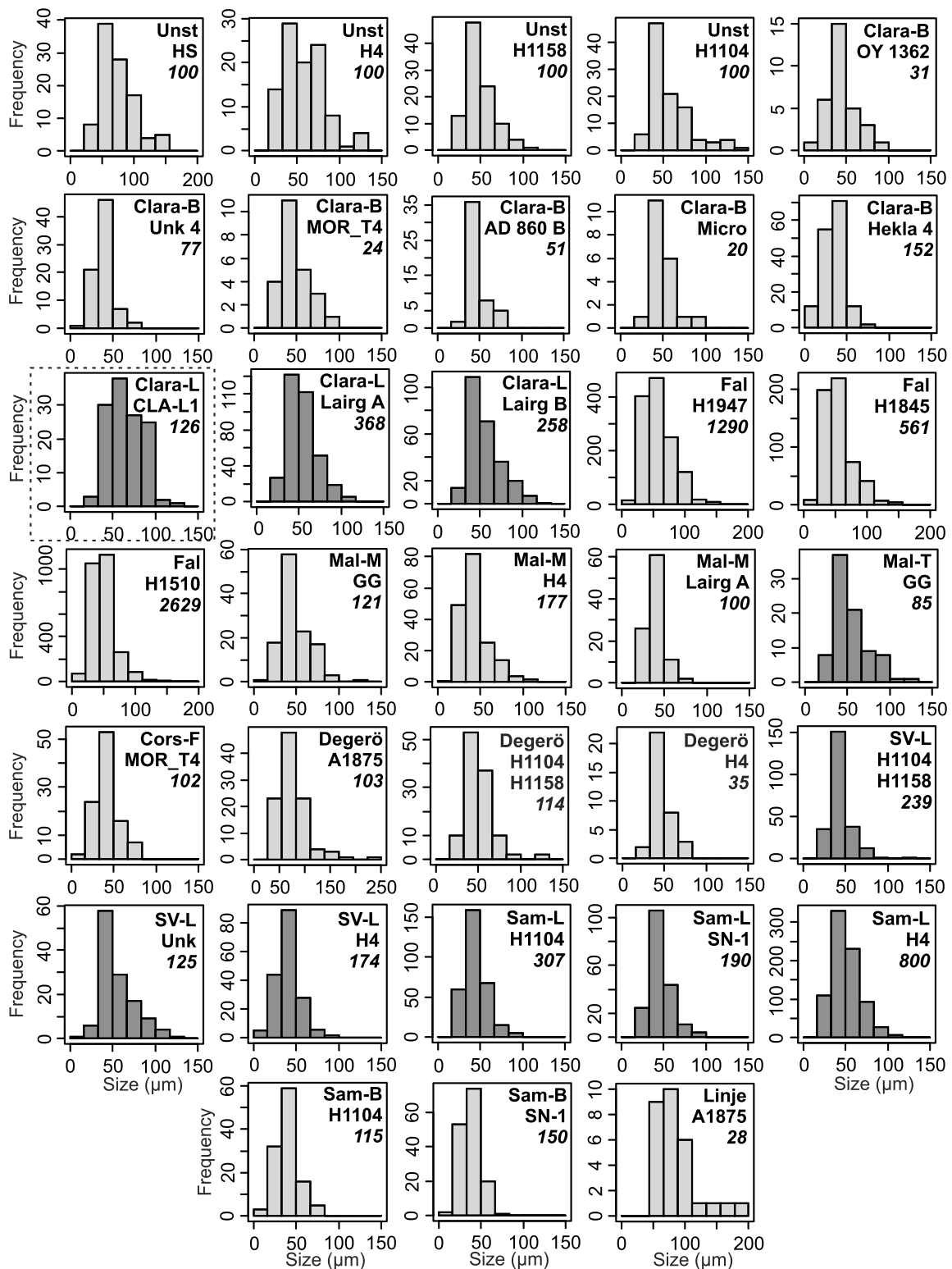


**Figure 3.** Histograms showing the distributions of shard size for cryptotephra at sites in the study. Lake samples are dark grey, and peatland samples are light grey. CLA-L1 is the only cryptotephra of basaltic composition to be included in this study and is highlighted by a dashed box. Abbreviations for cryptotephra deposits are as follows: H = Hekla, HS = Hekla Selsund, OY = Öraefajökull, Unk = Unknown, Micro = Microlite/GB4-150, GG = Glen Garry, A = Askja, SN-1 = Snæfellsjökull SN-1 tephra, CLA-L1 basaltic tephra from an eruption of the Grímsvötn volcano [Watson *et al.*, 2016]. Site names: Clara-B = Claraghmore peatland, Clara-L = Claraghmore lake, Fal = Fallahogy, Mal-M = Malham Moss, Mal-T = Malham Tarn, Cors-F = Cors Fochno, Degerö = Degerö Stormyr, SV-L = Lake Svartkälstjärn, Sam-L = Lake Sammakovuoma, Sam-B = Sammakovuoma bog. Only cryptotephra with >20 shards are plotted. The number of shards counted in each sample is shown in italics.

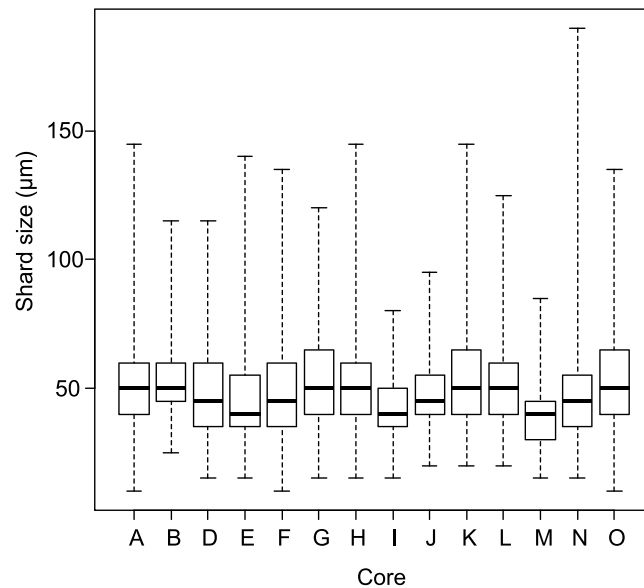


**Figure 4.** Shard size measurements for the Hekla 1510 cryptotephra taken from 14 cores from Fallahogy peatland [Watson *et al.*, 2015],  $n$  as follows: A = 199, B = 101, D = 176, E = 508, F = 163, G = 123, H = 96, I = 147, J = 145, K = 141, L = 119, M = 114, M = 204, O = 393.

distances (in this instance  $>1800$  km). However, large shards were relatively rare. Although 90% of particles were  $30\ \mu\text{m}$  or larger and 40% were over  $50\ \mu\text{m}$ , only 3% of shards were over  $100\ \mu\text{m}$ , suggesting that the majority of shards exceeding  $100\ \mu\text{m}$  in size fall out before reaching our sites. The only basaltic tephra included in this study (CLA-L1) does not display the same lognormal shard size distribution.

### 3.2. Aspect Ratio

Aspect ratio is a simple descriptor for predicting the terminal velocity of volcanic ash [Riley *et al.*, 2003]. The glass shards in this study predominantly had unequal max A and max B measurements, and aspect ratio ranged from 1.0 to 10.5. However, the majority of shards had a measured aspect ratio  $<3$  (Figure S4). Aspect ratio for all the Icelandic cryptotephtras studied here had a mean of 1.5.

## 4. Discussion

### 4.1. Records of Glass Shard Size Distributions in Lakes and Peatlands

#### 4.1.1. Hypothesis 1 (Shard Size Differs Between Peat Cores from the Same Site)

We examined the median size of shards from the Hekla 1510 cryptotephra, which were identified in 14 different cores at Fallahogy peatland (Figure 4). A minimum of 97 shards were examined in each core. There is a significant difference in the median shard size for different cores, with a range of values from 40 to  $50\ \mu\text{m}$  (Kruskal-Wallis,  $p < 0.0001$ ). Our results suggest that glass shards are differentially deposited, or reworked differentially, according to size. The degree of within-site variability in median shard size must be considered when making comparisons between sites (e.g., intrasite differences must be smaller than between-site differences). The 95th percentile values for shard size also show within-site variation, ranging from 62 to  $100\ \mu\text{m}$ .

#### 4.1.2. Hypothesis 2 (Shard Size Differs Between Lakes and Peatlands)

We analyze the shard size of five cryptotephtras in a lake and a peatland in close proximity. These cryptotephtras are selected because they appear in both a lake and a peatland in close proximity and  $>50$  shards have been measured in each tephra layer in both the lake sediments and peatland. In one instance (Glen Garry at Malham) the median shard size is identical in the lake and peatland (Figure 5). In all other instances, there is a significant difference between the median shard size in the cryptotephra deposits in peatlands and lakes (Mann-Whitney,  $p < 0.05$ ; Table S2). Where a significant difference is identified in three of four instances, median shard size was larger in the lake deposits than in peat. Except for one instance where the largest shard size was equal in both the peatland and the lake sediments, the largest shards were found in lakes, which in four instances also contain shard size distributions with a higher upper quartile shard size. However, these results must be interpreted with caution, given the intrasite variation identified in shard size within a tephra layer in a peatland (hypothesis 1). In some instances the differences between the shard size in lakes and peatlands are within the range which could be accounted for by intrasite variation in the peatland site. Nevertheless, the trend toward a greater amount of larger shards in lakes might be due to the possible in-wash of shards from across the catchment or within lake-basin redistribution. Although more intrasite lake and peatland cores would allow for a better understanding, from the available data, lakes appear to capture the largest shards to fall out over a region. Therefore, shard size data from small lakes may be more valuable in constraining maximum shard size for modeling studies than equivalent data from peatlands. For the

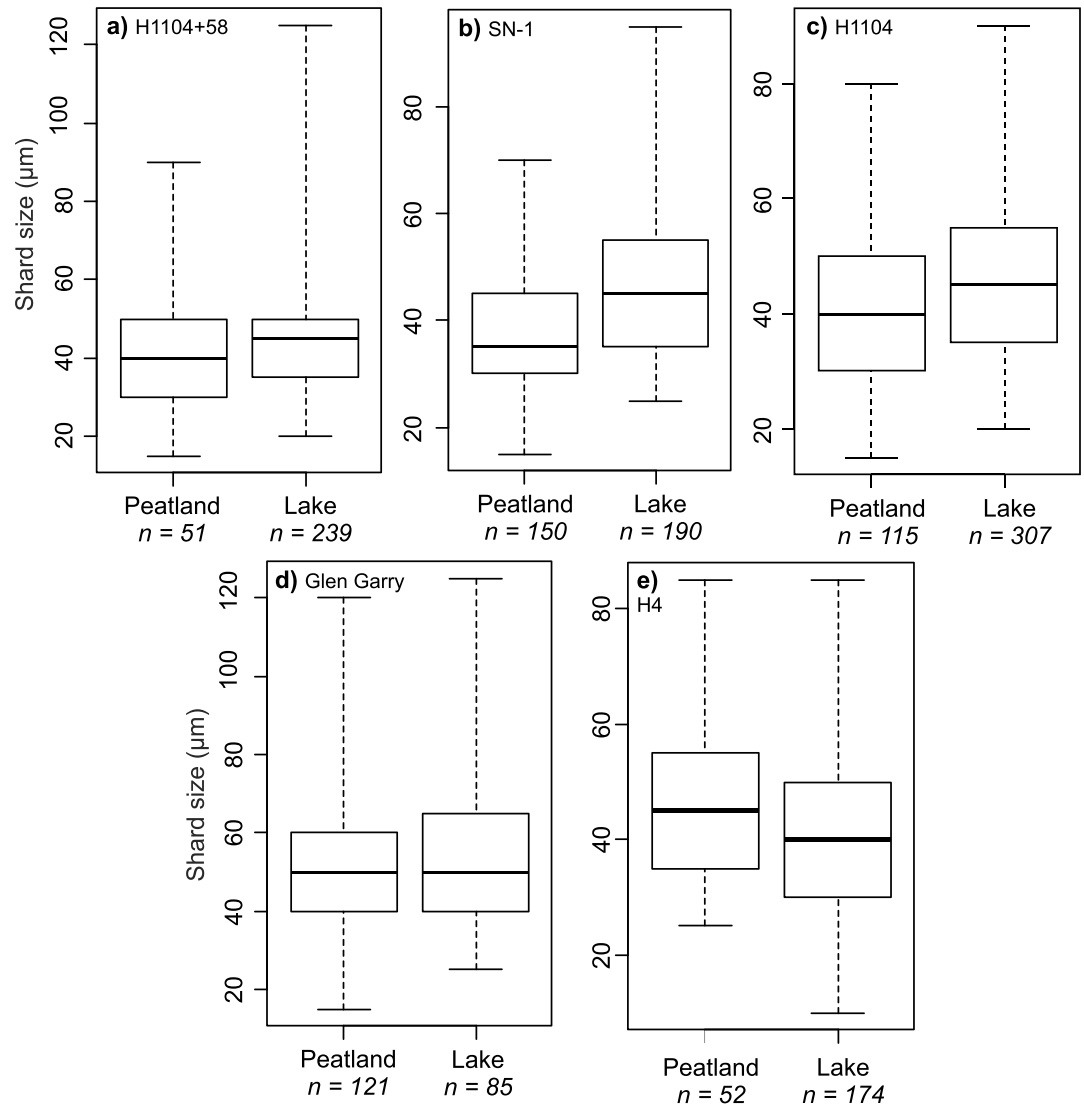


**Figure 5.** The shard size distribution for the same cryptotephra in peatland and lake sites which are in close proximity (<10 km apart). (a) Hekla 1104 and 1158 cryptotephra in Degerö Stormyr (peatland) and Svartkålstjärn lake, (b) SN-1 cryptotephra in Sammakovuoma lake and peatland, (c) Hekla 1104 cryptotephra in Sammakovuoma lake and peatland, (d) Glen Garry cryptotephra in Malham Moss and Malham Tarn, and (e) Hekla 4 cryptotephra in Sammakovuoma lake and peatland. Box plot convention is as follows: the boxes indicate the interquartile range, and the central line through each box indicates the median. The far extents of the upper and lower lines from each quartile indicate the maximum and minimum.

cryptotephra deposits at sites where aspect ratio data were available (Malham Tarn, Malham Moss, Lake Svartkålstjärn, and Degerö Stormyr), there was no significant difference in the median aspect ratio for the glass shards in lakes and peatlands, suggesting that fragmentation in the lake catchment has a negligible impact on glass shard morphology (Mann-Whitney,  $p < 0.05$ ; Table S3).

## 4.2. Vertical Movement of Shards

### 4.2.1. Hypothesis 3 (Shard Size Varies Vertically Within a Single Tephra Layer)

It has been shown that glass shards might be subject to differential vertical movement through peat profiles according to size, with smaller shards penetrating deeper [Payne and Gehrels, 2010]. However, plots of median shard size with depth in profile for the cryptotephtras identified in this study in both lakes and peatlands do not appear to display any coherent trend in size with depth in a tephra layer (Figure S5).

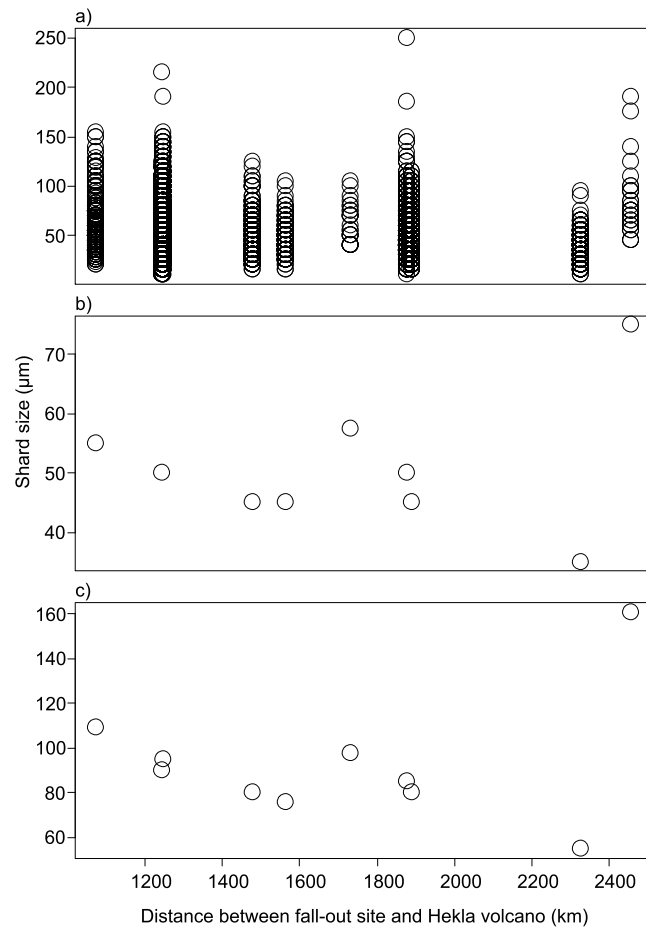


**Figure 6.** Shard size for all cryptotephra deposits identified in this study: (a) all data, (b) median values for each distance, and (c) 95th percentile values for each distance.

**4.3. Information from Particle Size Analysis**

**4.3.1. Hypothesis 4 (Shard Size Decreases with Distance from Source)**

When glass shard-size data from all cryptotephra deposits at all sites are combined there was only a weak correlation between median shard size and distance from Iceland (Spearman’s rank correlation:  $r = -0.127$ ,  $p < 0.0001$ ; Figure 6) over the range of distances covered by our sites (1075–2457 km). A trend toward fewer larger shards (lower 95th percentile values) is apparent with increased distance. However, there are still outliers, such as that relating to the Askja 1875 tephra which was identified at a distance of >2000 km in Poland but which has a median shard size of 75 µm. The intrasite differences in median shard size identified at Fallahogy (which ranged from 40 to 50 µm) must be considered when using shard size values from multiple sites to examine possible differences in size with distance from Iceland. However, the range of median shard size across all cryptotephra at all sites in this study was 35–75 µm, much greater than the intrasite differences identified at Fallahogy.

Owing to the patchy nature of tephra fallout, even cryptotephra deposits which form the most widespread iso-

chrons, for example the Hekla 4 tephra (2395–2279 B.C. [Lawson *et al.*, 2012]), are not present at every site. Therefore, the sample size for analysis of shard size with distance is reduced when focusing on tephra produced during one eruption. Two cryptotephra deposits, geochemically and stratigraphically correlated to the Hekla 4 and Hekla 1104 eruptions, were identified at six sites and five sites, respectively. Despite the range of distances where Hekla 4 cryptotephra was identified (~1000–1900 km), the median shard size varied across a relatively small range (35–55 µm; although still larger than the intrasite differences identified at Fallahogy). There is a significant positive correlation between shard size and distance from Hekla for the Hekla 4 cryptotephra (Spearman’s rank correlation:  $r = 0.170$ ,  $p < 0.0001$ ). This is contrary to the expectation that shard size would decrease with increasing distance from the volcano. This correlation is weak and is skewed by the most distal site (Sammakovuoma Lake) where the deposit has a relatively large median shard size of 50 µm (Figure 7). The 95th percentile for the shard size of the Hekla 4 cryptotephra is considerably greater (99 µm) at the site closest to Iceland (Unst, ~1000 km) than at sites in Ireland (60 µm, ~1200 km), England (75 µm, ~1500 km), and Sweden (70 µm and 80 µm, ~1900 km), although there still appears to be no simple relationship between shard size and distance from source (Figure 7).

There is a significant difference between shard size values for the Hekla 1104 cryptotephra from a peatland in Shetland ( $n = 102$ ) and at sites in Sweden (Sammakovuoma lake and peatland combined ( $n = 419$ ), Lake Svartkälstjärn, and Degerö Stormyr combined ( $n = 353$ )), supporting the hypothesis that shard size decreases with increasing distance from source (Kruskal-Wallis,  $p < 0.0001$ , median shard size for Shetland and two Swedish sites = 50 µm, 45 and 40 µm, respectively; Figure 8). The 95th percentile of shard

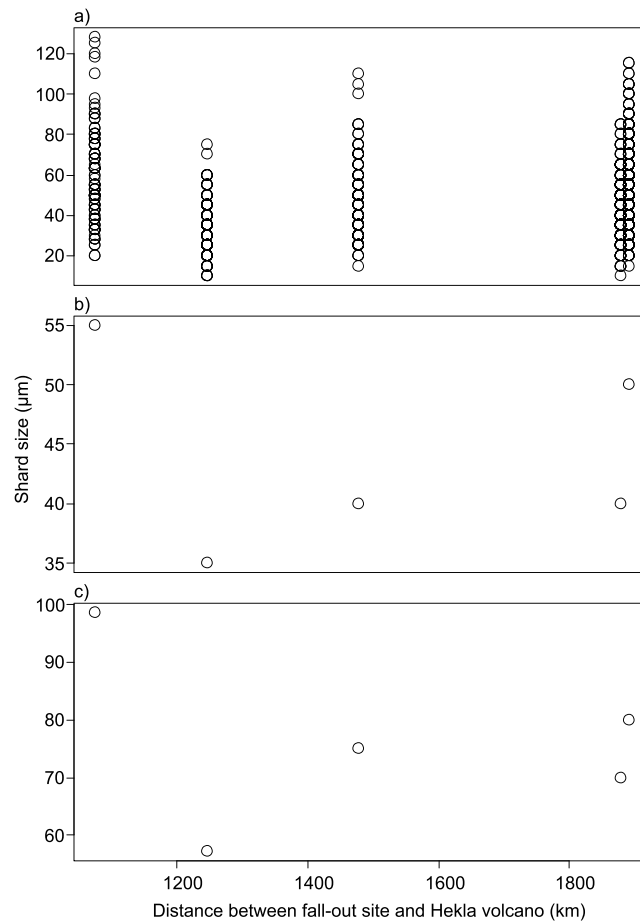


**Figure 7.** Shard size of the Hekla 4 cryptotephra identified at five sites across northern Europe: (a) all data, (b) median values for each distance, and (c) 95th percentile values for each distance.

size for Hekla 1104 is considerably larger (110 μm) in Unst, Shetland (~1000 km from Iceland) than that at sites in Sweden, 1900 km from Iceland (60–70 μm). Differences in the 95th percentile shard size with distance for both the Hekla 4 and Hekla 1104 eruptives indicate that larger shards are being lost as distance increases. Although this is not significantly impacting the median shard size, it is evident when the largest shards are considered.

There are various possible reasons for the strength and variety of correlations observed pertaining to changes in shard size with distance, even in tephra from a single eruption. First, the major controls on transport distance such as weather conditions, the height of the eruption column, tephra geochemistry (and thus mass), mass eruption rate, and degree of tephra fragmentation vary even during a single eruption [Carey et al., 2010; Gudmundsson et al., 2012], and in this instance the only true comparison would be between glass shards released during the same phase of an eruption. The hypothesis that tephra at different sites may have been deposited during different eruptive phases is supported by geochemical data. The geochemistry of the Hekla 4 cryptotephra varies at different sites in this study, reflecting geo-

chemical variation which has been identified in the proximal geological record where products of the Hekla 4 eruption show a range of geochemistry as the eruption progresses with SiO<sub>2</sub> content decreasing from approximately 74% to 57% [Larsen and Thorarinsson, 1977; Dugmore et al., 1995; Langdon and Barber, 2004] (Figure S6 data sources: Dugmore and Newton [1992], Dugmore et al. [1992], Boyle [1995], Dugmore et al. [1995], Pilcher et al. [1995], Pilcher et al. [1996], Dugmore and Newton [1998], Wastegård et al. [2001], Zillen et al. [2002], and Pilcher et al. [2005]). Deposits at some sites in this study (e.g., Sammakovuoma Lake) show glass shards with two distinct groups of Hekla 4 geochemistry, and hence, they may have received fallout on more than one occasion during the eruption. Changing weather conditions during eruptions can also influence tephra transport. Although detailed weather data are not available for many Holocene tephra, on the basis of observations of recent Icelandic eruptions, it is likely that tephra was transported over longer distances than the great circle distance between source and fallout site [Thorarinsson, 1981; Stevenson et al., 2013; Cooke et al., 2014]. Tephra may also be preferentially deposited during rainfall events [Langdon and Barber, 2004].

Another possible reason for the lack of strong correlation between shard size and distance is that glass shards may have aggregated and fallen out earlier than would be predicted based on their individual size [Durant et al., 2009]. Aggregate grains close to the volcano can be relatively large and composed of component shards with shard lengths in the range of those examined in this study (63–250 μm) [Taddeucci et al., 2011]. However, the examination of aggregate grains which travelled further and fell over the UK during the eruption of Eyjafjallajökull in 2010 shows that they are smaller (mean size 85 μm) and made up predominantly of glass shards <5 μm in diameter [Stevenson et al., 2012]. Such aggregate grains would have most

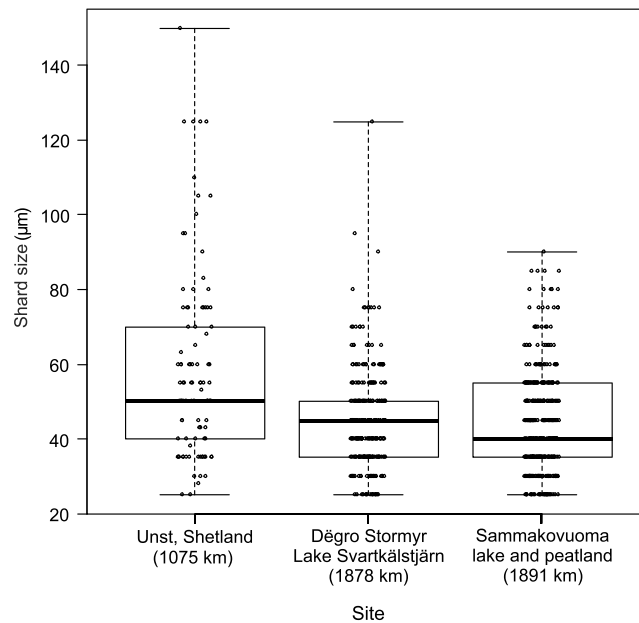


**Figure 8.** Box plots (with overlain jitter plot) of the shard size of the Hekla 1104 cryptotephra identified at sites in Sweden and Shetland. Distance displayed is the great circle distance between the Hekla volcano and fallout site. Box plot convention is as follows: the boxes indicate the interquartile range, and the central line through each box indicates the median. The far extents of the upper and lower lines from each quartile indicate the maximum and minimum. The hollow circles indicate the raw data values.

records lie within the fallout transport range of our modeled eruption parameters for Iceland. As our model does not account for aggregation, the fallout of individual small glass shards could be expected at these sites without the need to invoke aggregation or washout by precipitation.

The majority of the glass shards in the geological record fell out within the interquartile range of modeled transport distances. The most likely combination of input parameters to be sampled from the input probability distribution functions, and which results in a fallout distance within the interquartile range, is a plume height of approximately 10 km, wind speed of approximately  $17 \text{ ms}^{-1}$ , and a sphericity of 0.79. However, it is also possible that glass shards in the geological record were deposited during an eruption with a plume height as low as 4 km but where wind speeds were high ( $>20 \text{ ms}^{-1}$ ; Figure S7). This combination of input parameters is less likely to occur in the model as faster wind speeds are sampled less often. In agreement with the findings of *Beckett et al.* [2015], sphericity has less of an impact on modeled transport distance than either plume height or wind speed. Less spherical particles travel further; a  $30 \mu\text{m}$  nonspherical particle (sphericity of 0.45) will travel  $\sim 35\%$  further than a spherical particle of the same size.

Glass shards captured by rain gauge samples in the UK during the eruptions of Eyjafjallajökull 2010 and Grímsvötn 2011 display smaller shard sizes than those in cryptotephra deposits found in geological records [*Stevenson et al.*, 2012, 2013] (Figure 9). According to the model output, tephra that gave rise to the shard sizes identified in rain gauge samples are likely to have come from eruptions with lower plume heights and slower wind speeds when compared to glass shards we identify in the geological record in our study. In accordance with our model output, air mass trajectories indicate that although plume heights during Grímsvötn 2011 reached 20 km, only tephra from the lowest 4 km of the plume was transported toward the UK [*Stevenson et al.*, 2013].

Although our model can account for the median shard size in geological records in our study, in some instances it cannot account for the transport of the very largest shards over long distances. Below, we examine two examples to illustrate this point.

likely broken up (upon burial) in the geological record into constituent shards below the minimum sample size examined here ( $10 \mu\text{m}$ ). Therefore, premature fallout of glass shards by aggregation would appear unlikely to be the primary reason for our observations.

#### 4.3.2. Aspect Ratio

There is a significant correlation between increasing shard size and increasing aspect ratio (Spearman's rank correlation,  $r = 0.293$ ,  $p = <0.0001$ ). This finding is in agreement with the principle that nonspherical objects travel further in the atmosphere before deposition than spherical objects of the same size [*Rose et al.*, 2003]. However, it must be noted that aspect ratio as measured in this study assumes that glass shards present themselves with A and B axes parallel with the microscope slide.

#### 4.4. Comparing Model Output with the Geological Record

Figure 9 shows a summary of the model outputs for the setup detailed in Table 2. Data on shard size from geological

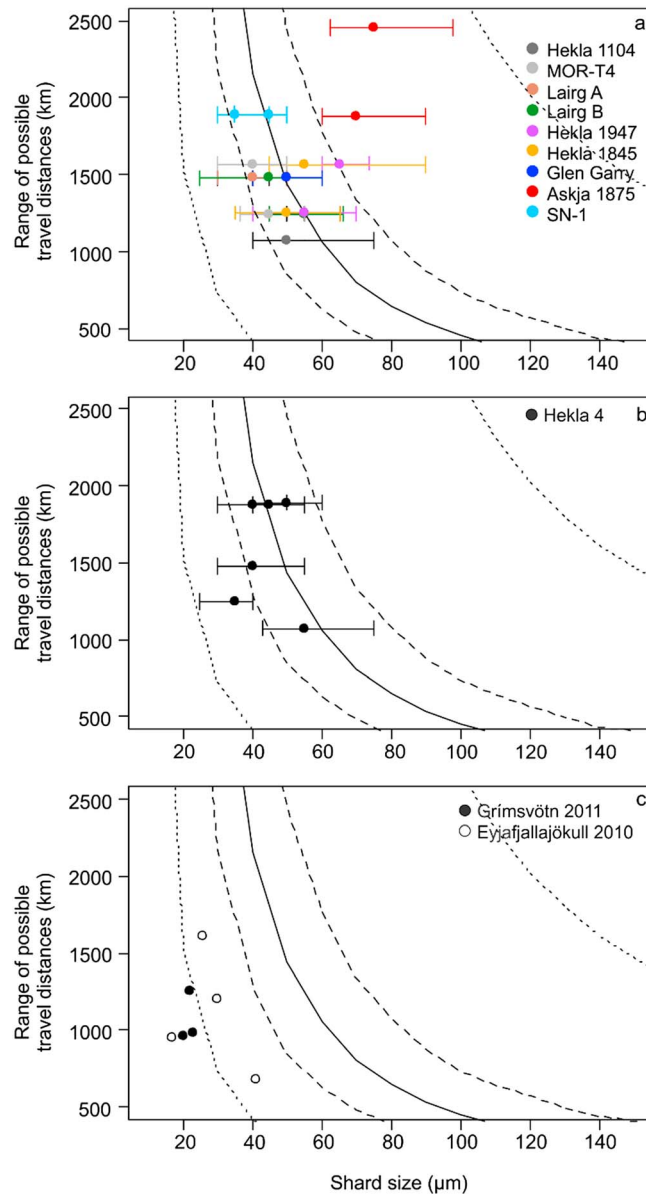


**Figure 9.** Model outputs for the setup detailed in Table 2 in comparison to cryptotephra in the geological record. The curved lines indicate a summary of model output (dotted lines = minimum and maximum, dashed lines = lower and upper quartiles, solid line = median value). The points show the median shard length, and the horizontal bars on all plots indicate the upper quartile and lower quartile values for shard size at each site. (a) Range of possible travel distances plotted against those travelled by all cryptotephra deposits identified at  $\geq 2$  sites in the geological record at sites in this study (excluding Hekla 4), (b) limited range of possible travel distances plotted against those travelled by tephra from the Hekla 4 eruption which was identified in the geological record as cryptotephra deposits at six sites in this study, and (c) limited range of possible travel distances plotted against those travelled by all glass shards collected from rain gauge samples [Stevenson et al., 2012, 2013].

shard size for the WRAe tephra identified in Newfoundland ( $73 \mu\text{m}$ ,  $n = 100$ ) [Pyne-O'Donnell et al., 2012]. Such small apparent differences in shard size with distance might be indicative of a “sweet spot,” whereby shards of a certain size and geometry are preferentially transported over long distances.

**4.4.1. Askja 1875 and the A.D. 860 B Tephra**

Askja 1875 is of special interest as glass shards identified in the geological record from this eruption are anomalously large when compared to shards from other eruptions. In Linje mire, northern Poland, 2500 km from the Askja crater, the median shard size for this cryptotephra is  $75 \mu\text{m}$  (maximum  $190 \mu\text{m}$ ,  $n = 28$ ). Under the set of eruption parameters in Table 2, our model does not predict the transport of glass shards of  $190 \mu\text{m}$  beyond  $\sim 1074$  km. However, the eruption parameters in Table 2 may not be suitable for the eruption of Askja 1875, which is estimated to have had a combination of high plume heights (26–37 km) and fast wind speeds (up to  $43 \text{ ms}^{-1}$ ) [Carey and Sparks, 1986; Carey et al., 2010]. Using these input parameters, the maximum predicted travel distance for a shard of  $190 \mu\text{m}$  is 1409 km, still much shorter than the 2500 km distance recorded in the geological record. In order to simulate the transport of particle of  $190 \mu\text{m}$  over 2500 km, a plume height of  $> 50$  km would need to be combined with a wind speed of  $43 \text{ ms}^{-1}$ . These eruption parameters would appear to be highly unlikely and are not supported by tephrostratigraphic data in Iceland.

Increasingly cryptotephra deposits are being linked to volcanoes further afield [Ponomareva et al., 2015]. An example is the “A.D. 860 B” tephra correlated to the White River Ash east (WRAe) from the Bona-Churchill massif, Alaska ( $61.38^\circ\text{N}$ ,  $141.75^\circ\text{W}$ ) [Jensen et al., 2014]. The median shard size for A.D. 860 B at Claraghmore peatland (6500 km distant) is  $45 \mu\text{m}$ , similar to the overall median shard size for all eruptions of an Icelandic source ( $50 \mu\text{m}$ ), despite the difference in transport distance of 5200 km. Furthermore, the maximum shard size for A.D. 860 B ( $n = 51$ ) at Claraghmore was  $75 \mu\text{m}$ , around the same size as the maximum

The Bona-Churchill massif eruption which produced the WRAe had a magnitude of VEI 6 based on an estimated eruptive volume of  $\sim 50 \text{ km}^3$  [Lerbekmo, 2008]. The maximum distance travelled by a  $75 \mu\text{m}$  shard (maximum shard size for A.D. 860 B,  $n=51$ ) based on a plume height of 40 km and a wind speed of  $30 \text{ ms}^{-1}$  in our simple model is 4600 km. It is possible that glass shards were transported in the polar jet stream (10–15 km height), which can reach speeds in excess of  $50 \text{ ms}^{-1}$  [Ahrens, 2012]. However, a particle released from 40 km which travels at a wind speed of  $30 \text{ ms}^{-1}$  and enters the jet stream from 10 to 15 km at a wind speed of  $50 \text{ ms}^{-1}$  is still transported only 5200 km. In these instances our model does not reproduce the evidence (maximum shard size) from the geological record.

## 5. Conclusions

We report the glass shard major element chemistry and examine shard size distributions for distal cryptotephra deposits at 14 sites across northern Europe and confirm the lognormal distribution of particle size identified in a small number of cryptotephra records by Stevenson *et al.* [2015].

We examine a number of hypotheses around the replicability and reliability of glass shard size measurements from ombrotrophic peatland and lake sediment archives. We identify no significant vertical sorting of shards within lake and peat sediments. Measuring the sizes of 100 shards from the vertical sample of peak shard concentration is generally sufficient to ascertain the median shard size for a cryptotephra deposit. Lakes and peatlands in close proximity contain cryptotephra deposits with significantly different median shard sizes in four out of five instances. Generally, lake sediments contain a greater number of larger shards than peatlands. We conduct an intrasite comparison of shard size and identify differences in the median shard size (which varied between 40 and  $50 \mu\text{m}$ ) with a peatland site. Intrasite differences must be taken into account when examining the differences in shard sizes between sites.

The range of median shard sizes (from 35 to  $75 \mu\text{m}$ ) varied more between all sites than the within-site variation displayed in our intrasite investigation, allowing for an examination of regional trends. When all cryptotephra deposits at all sites are considered, there is a weak but significant negative correlation between median shard size and distance of the fallout site from Iceland. However, in some instances (e.g., Hekla 4 cryptotephra) shard size appears to *increase* with distance from Iceland, possibly due to the deposition of tephra over different regions during different eruptive phases. Furthermore, the median shard size ( $45 \mu\text{m}$ ) of cryptotephra deposits from eruptions further afield (e.g., Alaska) is not dissimilar to that of cryptotephra deposits from Iceland ( $50 \mu\text{m}$ ), despite a difference of  $\sim 5200 \text{ km}$  in transport distance. When combined with uncertainties about wind speed during ancient eruptions, this similarity makes refining possible tephra source regions based on shard size challenging and reinforces the need to use chemical data for shards as well as grain size.

The median shard size of cryptotephra deposits in the geological record in our study generally lies within the interquartile range of predicted transport distances from our probabilistic model, indicating that the assumed input probability distributions are reasonable. However, our model is not able to account for the transport distance of some large shards.

This paper indicates the potential for using cryptotephra shard size to inform our understanding of past eruptions, and the particle size data set presented here provides an important resource for testing models of ash dispersal over northern Europe.

## Acknowledgments

This research was undertaken while Elizabeth Watson held a NERC-funded Doctoral Training grant (NE/K500847/1). The authors would like to acknowledge Mariusz Lamentowicz for supplying core material from two sites in Poland. The data used in this manuscript are listed in the references, tables, and supporting information.

## References

- Ahrens, C. D. (2012), *Meteorology Today: An Introduction to Weather, Climate, and the Environment*, Cengage Learning, Canada.
- Alfano, F., C. Bonadonna, P. Delmelle, and L. Costantini (2011), Insights on tephra settling velocity from morphological observations, *J. Volcanol. Geotherm. Res.*, *208*, 86–98, doi:10.1016/j.jvolgeores.2011.09.013.
- Beckett, F., C. Witham, M. Hort, J. Stevenson, C. Bonadonna, and S. Millington (2015), Sensitivity of dispersion model forecasts of volcanic ash clouds to the physical characteristics of the particles, *J. Geophys. Res. Atmos.*, *120*, 636–652, doi:10.1002/2015JD023609.
- Blockley, S. P. E., S. D. F. Pyne-O'Donnell, J. J. Lowe, I. P. Matthews, A. Stone, A. M. Pollard, C. S. M. Turney, and E. G. Molyneux (2005), A new and less destructive laboratory procedure for the physical separation of distal glass tephra shards from sediments, *Quat. Sci. Rev.*, *24*, 1952–1960, doi:10.1016/j.quascirev.2004.12.008.
- Bonadonna, C., and J. C. Phillips (2003), Sedimentation from strong volcanic plumes, *J. Geophys. Res.*, *108*(B7), 2340, doi:10.1029/2002JB002034.
- Bonadonna, C., C. B. Connor, B. Houghton, L. Connor, M. Byrne, A. Laing, and T. Hincks (2005), Probabilistic modeling of tephra dispersal: Hazard assessment of a multiphase rhyolitic eruption at Tarawera, New Zealand, *J. Geophys. Res.*, *110*, B03203, doi:10.1029/2003JB002896.
- Boyle, J. E. (1995), Tephra in lake sediments: An unambiguous geochronological marker?, PhD, Univ. of Edinburgh.

- Brown, R. J., C. Bonadonna, and A. J. Durant (2012), A review of volcanic ash aggregation, *Phys. Chem. Earth, Parts A/B/C*, 45–46, 65–78, doi:10.1016/j.pce.2011.11.001.
- Carey, R. J., B. F. Houghton, and T. Thordarson (2010), Tephra dispersal and eruption dynamics of wet and dry phases of the 1875 eruption of Askja Volcano, Iceland, *Bull. Volcanol.*, 72, 259–278, doi:10.1007/s00445-009-0317-3.
- Carey, S. N., and H. Sigurdsson (1982), Influence of particle aggregation on deposition of distal tephra from the May 18, 1980, eruption of Mount St. Helens volcano, *J. Geophys. Res.*, 87, 7061–7072, doi:10.1029/JB087iB08p07061.
- Carey, S., and R. S. J. Sparks (1986), Quantitative models of the fallout and dispersal of tephra from volcanic eruption columns, *Bull. Volcanol.*, 48, 109–125, doi:10.1007/BF01046546.
- Connor, C. B., L. J. Connor, C. Bonadonna, J. Luhr, I. P. Savov, and C. Navarro-Ochoa (2013), Modeling tephra thickness and particle size distribution of the 1913 eruption of Volcán de Colima, Mexico, in *Volcan de Colima, Spec. Publ.*, edited by N. Varley, Geol. Soc. of Am. Springer-Verlag, Berlin, isbn:978-3-642-25911-1.
- Cooke, M. C., P. N. Francis, S. Millington, R. Saunders, and C. Witham (2014), Detection of the Grímsvötn 2011 volcanic eruption plumes using infrared satellite measurements, *Atmos. Sci. Lett.*, 15, 321–327, doi:10.1002/asl2.506.
- Davies, S. M., M. Elmquist, J. Bergman, B. Wohlfarth, and D. Hammarlund (2007), Cryptotephra sedimentation processes within two lacustrine sequences from west central Sweden, *Holocene*, 17, 319–330, doi:10.1177/0959683607076443.
- De Vleeschouwer, F., F. M. Chambers, and G. T. Swindles (2011), Coring and sub-sampling of peatlands for palaeoenvironmental research, *Mires Peat*, 7, 1–10.
- Dugmore, A. J., and A. J. Newton (1992), Thin tephra layers in peat revealed by X-radiography, *J. Archaeol. Sci.*, 19, 163–170, doi:10.1016/0305-4403(92)90047-7.
- Dugmore, A. J., and A. J. Newton (1998), Holocene tephra layers in the Faroe Islands, *Froðskaparrít.*, 46, 191–204.
- Dugmore, A. J., A. J. Newton, D. E. Sugden, and G. Larsen (1992), Geochemical stability of fine-grained silicic Holocene tephra in Iceland and Scotland, *J. Quat. Sci.*, 7, 173–183.
- Dugmore, A. J., G. Larsen, and A. J. Newton (1995), Seven tephra isochrones in Scotland, *Holocene*, 5, 257–266, doi:10.1177/095968369500500301.
- Durant, A. J., W. I. Rose, A. M. Sarna-Wojcicki, S. Carey, and A. C. M. Volentik (2009), Hydrometeor-enhanced tephra sedimentation: Constraints from the 18 May 1980 eruption of Mount St. Helens, *J. Geophys. Res.*, 114, B03204, doi:10.1029/2008JB005756.
- Folch, A. (2012), A review of tephra transport and dispersal models: Evolution, current status, and future perspectives, *J. Volcanol. Geotherm. Res.*, 235, 96–115, doi:10.1016/j.jvolgeores.2012.05.020.
- Ganser, G. H. (1993), A rational approach to drag prediction of spherical and nonspherical particles, *Powder Tech.*, 77, 143–152.
- Gudmundsson, M. T., et al. (2012), Ash generation and distribution from the April–May 2010 eruption of Eyjafjallajökull, Iceland, *Sci. Rep.*, 2, doi:10.1038/srep00572.
- Hall, M., C. Hayward (2014), *Preparation of micro- and crypto-tephras for quantitative microbeam analysis, Spec. Publ.*, vol. 398, pp. 21–28, Geol. Soc., London, doi: 10.1144/SP398.5.
- Hall, V. A., and J. R. Pilcher (2002), Late-Quaternary Icelandic tephra in Ireland and Great Britain: Detection, characterization and usefulness, *Holocene*, 12, 223–230, doi:10.1191/0959683602hl538rr.
- Hayward, C. (2012), High spatial resolution electron probe microanalysis of tephra and melt inclusions without beam-induced chemical modification, *Holocene*, 22, 119–125, doi:10.1177/0959683611409777.
- Jensen, B. J. L., et al. (2014), Transatlantic distribution of the Alaskan White River Ash, *Geology*, 42, 875–878, doi:10.1130/G35945.1.
- Jowsey, P. (1966), An improved peat sampler, *New Phytol.*, 65, 245–248.
- Lacasse, C. (2001), Influence of climate variability on the atmospheric transport of Icelandic tephra in the subpolar North Atlantic, *Global Planet. Change*, 29, 31–55, doi:10.1016/S0921-8181(01)00099-6.
- Lane, C. S., B. T. Chorn, and T. C. Johnson (2013), Ash from the Toba supereruption in Lake Malawi shows no volcanic winter in East Africa at 75 ka, *Proc. Natl. Acad. Sci. U. S. A.*, 110, 8025–8029, doi:10.1073/pnas.1301474110.
- Langdon, P. G., and K. E. Barber (2004), Snapshots in time: Precise correlations of peat-based proxy climate records in Scotland using mid-Holocene tephra, *Holocene*, 14, 21–33, doi:10.1191/0959683604hl686rp.
- Larsen, G., and S. Thorarinsson (1977), Hekla 4 and other acidic Hekla tephra layers, *Jökull*, 27, 28–46.
- Lawson, I. T., G. T. Swindles, G. Plunkett, and D. Greenberg (2012), The spatial distribution of Holocene cryptotephra in north-west Europe since 7 ka: Implications for understanding ash fall events from Icelandic eruptions, *Quat. Sci. Rev.*, 41, 57–66, doi:10.1016/j.quascirev.2012.02.018.
- Le Maitre, R. W., P. Bateman, A. Dudek, J. Keller, J. Lameyre, M. Le Bas, P. Sabine, R. Schmid, H. Sorensen, and A. Streckeisen (1989), *A classification of igneous rocks and glossary of terms: Recommendations of the International Union of Geological Sciences Subcommittee on the Systematics of Igneous Rocks*, Blackwell, Oxford.
- Lerbekmo, J. F. (2008), The White River Ash: Largest Holocene Plinian tephra, *Can. J. Earth Sci.*, 45, 693–700, doi:10.1139/E08-023.
- Lowe, D. J. (2011), Tephrochronology and its application: A review, *Quat. Geochronol.*, 6, 107–153, doi:10.1016/j.quageo.2010.08.003.
- Mattsson, S., and R. Vesanen (1988), Patterns of Chernobyl fallout in relation to local weather conditions, *Environ. Int.*, 14, 177–180, doi:10.1016/0160-4120(88)90092-X.
- Newhall, C. G., and S. Self (1982), The volcanic explosivity index (VEI): An estimate of explosive magnitude for historical volcanism, *J. Geophys. Res.*, 87, 1231–1238, doi:10.1029/JC087iC02p01231.
- Newton, A. J., A. J. Dugmore, and B. M. Gittings (2007), TephraBase: Tephrochronology and the development of a centralised European database, *J. Quat. Sci.*, 22, 737–743, doi:10.1002/jqs.1094.
- Payne, R., and M. Gehrels (2010), The formation of tephra layers in peatlands: An experimental approach, *Catena*, 81, 12–23, doi:10.1016/j.catena.2009.12.001.
- Pilcher, J. R., V. A. Hall, and F. G. McCormac (1995), Dates of Holocene Icelandic volcanic eruptions from tephra layers in Irish peats, *Holocene*, 5, 103–110.
- Pilcher, J. R., V. A. Hall, and F. G. McCormac (1996), An outline tephrochronology for the Holocene of the north of Ireland, *J. Quat. Sci.*, 11, 485–494.
- Pilcher, J., R. S. Bradley, P. Francus, and L. Anderson (2005), A Holocene tephra record from the Lofoten Islands, Arctic Norway, *Boreas*, 34, 136–156, doi:10.1111/j.1502-3885.2005.tb01011.x.
- Ponomareva, V., M. Portnyagin, and S. M. Davies (2015), Tephra without borders: Far-reaching clues into past explosive eruptions, *Front. Earth Sci.*, 3, 83, doi:10.3389/feart.2015.00083.
- Pyne-O'Donnell, S. D. F., et al. (2012), High-precision ultra-distal Holocene tephrochronology in North America, *Quat. Sci. Rev.*, 52, 6–11.
- Riley, C. M., W. I. Rose, G. J. S. Bluth (2003), Quantitative shape measurements of distal volcanic ash, *J. Geophys. Res.*, 108(B10), 2504, doi:10.1029/2001JB000818.

- Rose, W. I., and A. J. Durant (2011), Fate of volcanic ash: Aggregation and fallout, *Geology*, *39*, 895–896, doi:10.1130/focus092011.1.
- Rose, W., C. Riley, and S. Dartevelle (2003), Sizes and shapes of 10-Ma distal fall pyroclasts in the Ogallala Group, Nebraska, *J. Geol.*, *111*, 115–124, doi:10.1086/344668.
- Simkin, T., and L. Siebert (1994), *Volcanoes of the World: A Regional Directory, Gazetteer, and Chronology of Volcanism During the Last 10,000 Years*, Geosci. Press, Tucson, Ariz.
- Stevenson, J. A., et al. (2012), Distal deposition of tephra from the Eyjafjallajökull 2010 summit eruption, *J. Geophys. Res.*, *117*, B00C10, doi:10.1029/2011JB008904.
- Stevenson, J. A., S. Loughlin, A. Font, G. W. Fuller, A. MacLeod, L. W. Oliver, B. Jackson, C. J. Horwell, T. Thordarson, and I. Dawson (2013), UK Monitoring and deposition of tephra from the May 2011 eruption of Grimsvotn, Iceland, *J. Appl. Volcanol.*, *2*, doi:10.1186/2191-5040-2-3.
- Stevenson, J., S. Millington, F. Beckett, G. T. Swindles, and T. Thordarson (2015), Big grains go far: Reconciling tephrochronology with atmospheric measurements of volcanic ash, *Atmos. Meas. Tech. Discuss.*, *8*, 65–120, doi:10.5194/amt-8-2069-2015.
- Swindles, G. T., F. De Vleeschouwer, and G. Plunkett (2010), Dating peat profiles using tephra: Stratigraphy, geochemistry and chronology, *Mires Peat*, *7*, 1–9.
- Swindles, G. T., I. T. Lawson, I. P. Savov, C. B. Connor, and G. Plunkett (2011), A 7000 yr perspective on volcanic ash clouds affecting northern Europe, *Geology*, *39*, 887–890, doi:10.1130/G32146.1.
- Swindles, G. T., et al. (2013a), Re-deposited cryptotephra layers in Holocene peats linked to anthropogenic activity, *Holocene*, *23*, 1493–1501, doi:10.1177/0959683613489586.
- Swindles, G. T., I. P. Savov, C. B. Connor, J. Carrivick, E. J. Watson, and I. T. Lawson (2013b), Volcanic ash clouds affecting northern Europe: The long view, *Geol. Today*, *29*, 214–217.
- Taddeucci, J., P. Scarlato, C. Montanaro, C. Cimarelli, E. Del Bello, C. Freda, D. Andronico, M. T. Gudmundsson, and D. B. Dingwell (2011), Aggregation-dominated ash settling from the Eyjafjallajökull volcanic cloud illuminated by field and laboratory high-speed imaging, *Geology*, *39*, 891–894, doi:10.1130/G32016.1.
- Thorarinsson, S. (1981), Greetings from Iceland. Ash-falls and volcanic aerosols in Scandinavia, *Geografiska Annaler. Series A. Phys. Geogr.*, *63*, 109–118.
- Wastegård, S., S. Björck, M. Grauert, and G. E. Hannon (2001), The Mjauvotn tephra and other Holocene tephra horizons from the Faroe Islands: A link between the Icelandic source region, the Nordic Seas, and the European continent, *Holocene*, *11*, 101–109.
- Watson, E. J. (2016), Using cryptotephra layers to understand volcanic ash clouds, PhD Thesis, Univ. of Leeds.
- Watson, E. J., G. T. Swindles, I. T. Lawson, and I. P. Savov (2015), Spatial variability of tephra and carbon accumulation in a Holocene peatland, *Quat. Sci. Rev.*, *124*, 248–264, doi:10.1016/j.quascirev.2015.07.025.
- Watson, E. J., G. T. Swindles, I. T. Lawson, and I. P. Savov (2016), Do peatlands or lakes provide the most comprehensive distal tephra records?, *Quat. Sci. Rev.*, *139*, 110–128, doi:10.1016/j.quascirev.2016.03.011.
- Zillen, L. M., S. Wastegård, and I. F. Snowball (2002), Calendar year ages of three mid-Holocene tephra layers identified in varved lake sediments in west central Sweden, *Quat. Sci. Rev.*, *21*, 1583–1591.